PHYSICAL REVIEW B **96**, 184405 (2017)

Radiation damping in ferromagnetic resonance induced by a conducting spin sink

Mohammad M. Qaid,[1] Tim Richter,[1] Alexander Müller,[1] Christoph Hauser,[1] Camillo Ballani,[1] and Georg Schmidt[1,2,*]

[1]*Institut für Physik, Martin-Luther-Universität Halle-Wittenberg, Von-Danckelmann-Platz 3, 06120 Halle, Germany*

[2]*Interdisziplinäres Zentrum für Materialwissenschaften, Martin-Luther-Universität Halle-Wittenberg, Heinrich Damerow Straße 4, 06120 Halle, Germany*

(Received 18 July 2017; revised manuscript received 22 September 2017; published 6 November 2017)

We have investigated the damping in the ferromagnetic resonance (FMR) of yttrium iron garnet (YIG) caused by spin pumping into adjacent conducting materials, namely, Pt and the conducting polymer poly(3,4-ethylenedioxythiophene):poly(4-styrenesulfonate) (PEDOT:PSS). By a systematic study which also includes multilayers in which the conducting layer is separated from YIG by an insulator, we can show that a considerable part of the damping can be attributed to the so-called radiation damping which originates from the interaction of the magnetic fields caused by the precessing magnetization with the conducting layer. Especially, when PEDOT:PSS is used as a spin sink, the observed damping must be attributed completely to radiation damping, and no contribution from spin pumping can be identified. These results demonstrate that the Gilbert damping as a measure of spin pumping can only be used when careful control experiments accompany the investigation.

DOI: 10.1103/PhysRevB.96.184405

I. INTRODUCTION

Spin pumping describes the flow of a spin current from a ferromagnet into an adjacent material due to spin precession or due to thermal gradients in the ferromagnet [1,2]. When the spin current flows into a material with spin-orbit coupling, it can be converted into a charge current by the so-called inverse spin Hall effect (ISHE). The latter also is called spin-charge conversion and has been discussed, for example, for energy harvesting by converting temperature gradients into charge current [2–4]. Both spin pumping and inverse spin Hall effect have been investigated for a number of years. Only recently the inverse spin Hall effect also was reported for organic materials [5,6], a compelling result because organic conductors usually are expected to have little spin-orbit coupling and thus should show a very small ISHE if any at all. Because of low-cost fabrication methods and flexibility, however, organic materials would be very interesting candidates for spintronics especially as spin-charge converters in the above-mentioned applications. To investigate the process of spin pumping, however, not only can the inverse spin Hall effect be used, but also the damping in ferromagnetic resonance can be used as a measure for spin pumping because it is increased when spin current resulting from spin pumping flows into a material in which spin flip can take place, an effect which is often used for the quantification of spin pumping in literature [7,8].

Spin pumping transfers a pure spin current from a ferromagnet (FM) into a nonmagnetic conductor. In this process the precession of magnetization in the ferromagnetic layer in the FMR results in a nonequilibrium spin accumulation which can diffuse into the nonmagnet. This spin accumulation has a time-independent component which is collinear to the external bias field of the FMR and a time-dependent precessing component which is perpendicular. If the spin accumulation created in the nonmagnet experiences sufficient spin flip, it does not flow back into the ferromagnetic material, and the out diffusion of the spin current reduces the spin accumulation in the FM. As a result, the FM is closer to equilibrium, a fact which becomes visible as an enhanced damping and an increased linewidth in the FMR [1,7–9].

The process of spin pumping due to the magnetic precession and the associated damping enhancement is described by the Lindau-Lifshitz-Gilbert equation, Fig. 2(a). This equation describes the magnetization dynamics $M(t)$ in a ferromagnetic film under an effective magnetic field,

$$\frac{dM(t)}{dt} = -\gamma M(t) \times H_{\text{eff}} + \frac{\alpha}{M_s} M(t) \times \frac{dM(t)}{dt}, \quad (1)$$

where γ, α, and M_s are the gyromagnetic ratio, the Gilbert damping constant, and the saturation magnetization, respectively.

The fact that the spin pumping in an FM/normal-metal (NM) bilayer structure is investigated by the enhancement of the damping α in the FMR by a contribution α_{sp} caused by spin pumping is very common [1,10,11]. However, it has been found that, in addition to the intrinsic damping α_{in} and the contribution by spin-pumping α_{sp} [10,12–15], other damping sources also can have a significant contribution to the overall damping which may become dominant depending on the layers' structure, sample and waveguide dimensions, and experimental parameters and conditions. These damping sources include: eddy current damping α_{eddy} [12,16–18] radiative damping α_{rad} [19–21], and electromagnetic shielding damping α_{sh} [22–24].

In this paper, we have performed ferromagnetic resonance experiments on various structures based on YIG/PEDOT:PSS and YIG/Pt. Many steps and control experiments were performed to precisely investigate the resulting magnetic damping and its origins.

II. EXPERIMENTAL DETAILS

Sample fabrication

All measurements in this paper are performed on a series of layer structures based on 200-nm-thick films of single-crystal $Y_3Fe_5O_{15}$ (YIG) with dimensions $\sim(2\times5\,\text{mm}^2)$ grown on gadolinium gallium garnet (GGG) by liquid phase epitaxy.

*Author to whom correspondence should be addressed: georg.schmidt@physik.uni-halle.de

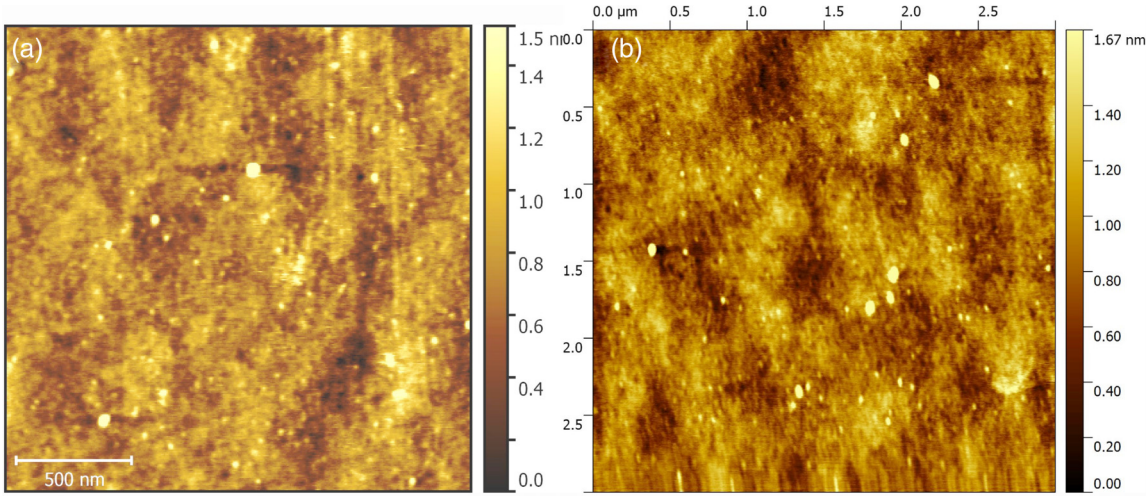

FIG. 1. AFM for the YIG (200-nm) surface at two different wafer areas.

All samples discussed are cut from the same YIG/GGG wafer. The surface quality and the roughness of these samples are investigated by atomic force microscopy (AFM). The rms surface roughness of YIG is 0.28 nm. Figures 1(a) and 1(b) show AFM images of the YIG surface.

For the investigation of spin pumping, two sample categories have been prepared using two different materials as spin sinks. One set of samples uses Pt deposited by magnetron sputtering for which the thickness was obtained by calibrating the growth rate using x-ray reflectometry. Another set uses highly doped poly(3,4-ethylenedioxythiophene):poly(4-styrenesulfonate) (PEDOT:PSS) which is a conducting polymer/organic conductor (OC). For deposition a suspension of 94.5 wt% of PEDOT:PSS is deposited by spin coating using a commercially available formulation in water (Clevios PH510, Heraeus) which is additionally doped with 5 wt% of dimethyl sulfoxide (DMSO). The nominal conductivity of the material is 300 S/cm. By doping with DMSO it can be enhanced substantially. A small amount of Dynole 0.5 wt% is added to the mixture as a surfactant to reduce the surface dynamic tension during spin coating. The solution is spin coated in ambient atmosphere at 4000 rpm for 1 min. The films are heated on a hot plate at 140 °C for 10 min. The resulting PEDOT:PSS has a thickness of 140 nm and an in-plane conductivity of $\sigma_{\text{in plane}} = 560\,\text{S}\,\text{cm}^{-1}$. The thickness is measured using a DEKTAK surface profilometer. Prior to the PEDOT:PSS or Pt deposition, the YIG surface is cleaned for 10 min using ultrasonic agitation in acetone, isopropyl alcohol, and de-ionized water, respectively.

For control experiments, an additional Al_2O_3 interfacial layer with a 30-nm thickness is deposited on some samples by thermal evaporation while directly measuring the thickness using a quartz microbalance. The layers and thicknesses of all samples are listed in Table I.

TABLE I. Samples used with materials and layer thicknesses.

Sample	YIG (nm)	Al_2O_3 (nm)	Pt (nm)	PEDOT:PSS (nm)
S1	200			
S2	200			140
S3	200		10	
S1	200	30		
S5	200	30		140
S6	200	30	5	
S7	200	30	10	
S8	200	30	15	
S9	200	30	20	

III. EXPERIMENTAL SETUP

A. Magnetic damping and ferromagnetic resonance

The primary goal of the experiments was to determine the spin-mixing conductance for YIG/PEDOT:PSS by measuring the difference in FMR damping for pure YIG and a YIG/PEDOT:PSS bilayer. Special emphasis was to be put on the identification of artifacts because a low spin-mixing conductance is to be expected for the interface to the polymer. To check the validity of the experiments a comparison with YIG/Pt should be performed. For the various experiments, the FMR is measured for all samples, and the damping enhancement with respect to pure YIG is extracted from the spectra. For the FMR measurements, the samples are placed face down on a stripline antenna. While an external homogeneous magnetic field (H_{ex}) fixes the magnetization of YIG parallel to the antenna, a radio-frequency (rf) current through the antenna is used to create an rf field (h_{rf}) which excites the ferromagnetic resonance in YIG [Fig. 2(a)]. The spectrum is taken by varying the external field.

The resolution of the field control is around 0.05 Oe. H_{ex} is modulated at a low amplitude at a frequency of 184 Hz allowing for measurements using a lock-in amplifier. rf is generated using a RHODE & SCHWARZ SMF100A Microwave Signal Generator. To determine the FMR amplitude the absorption in the waveguide is measured using a Schottky diode whose signal is fed into a lock-in amplifier. The output signal of the lock-in amplifier is measured using an Agilent 34420A 7.5 digit nanovoltmeter. The relative excitation power in these experiments is kept in the range between -1 and -10 dBm.

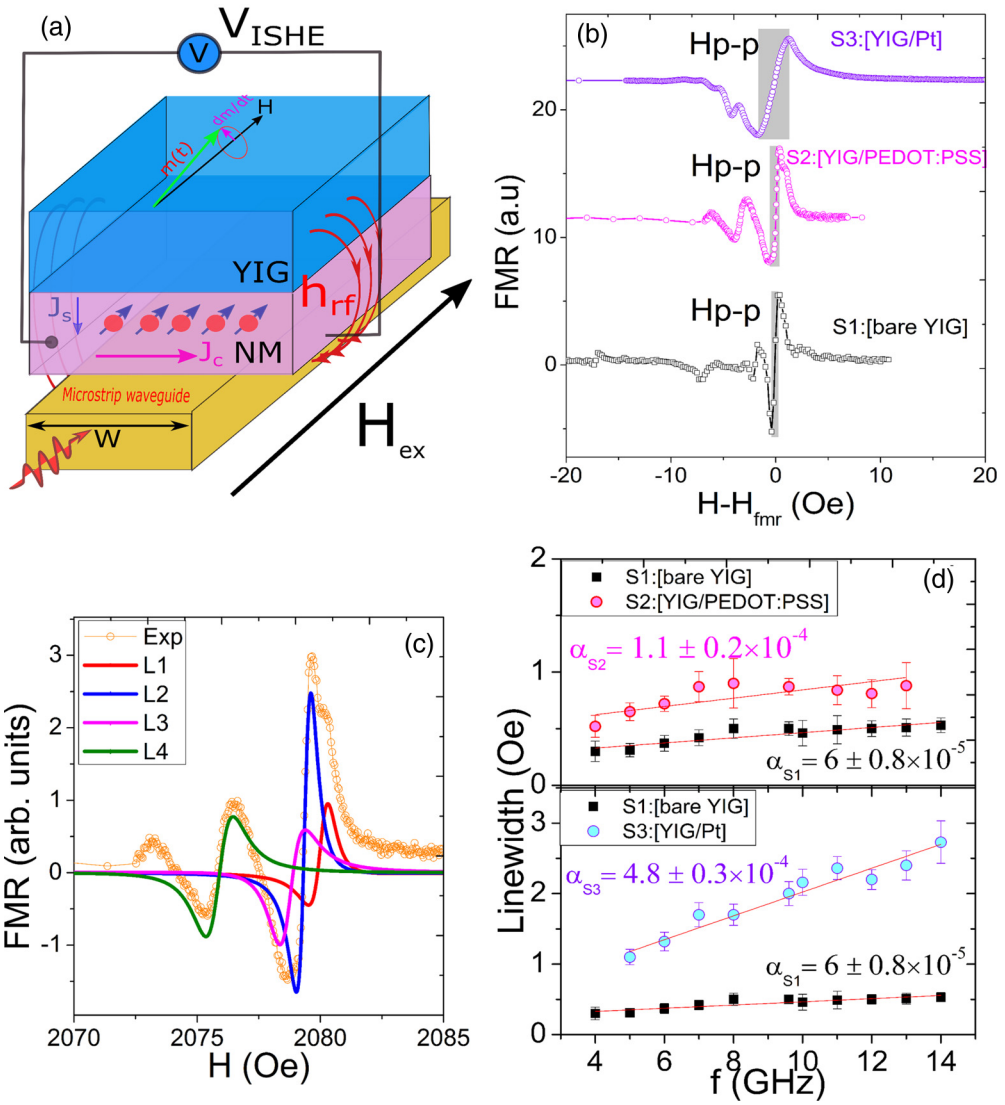

FIG. 2. (a) Schematic or the measurement geometry for the FMR and ISHE. (b) The FMR curves and linewidths obtained at 8 GHz for S1–S3. (c) The FMR curves showing the multiple lines in the spectrum for S2:[YIG-PEDOT:PSS]. The spectrum is taken with the in-plane magnetic field at a frequency of 8 GHz. The solid lines are fitted to Lorentzian line shapes. (d) The FMR linewidth as a function of the resonance frequency. The damping values for S1–S3 are determined from the slope of the linear fit. The errors for the damping values are estimated from the standard error resulting from the linear fit. The errors for the linewidth values are estimated considering both the magnetic-field modulation 0.05 Oe and the deviation of the FMR Lorentz fit from the experimental data.

Due to the lock-in measurement the measured signal represents not the absorption signal but its derivative.

Gilbert damping is obtained using the FMR linewidth frequency dependence of the uniform mode. The linewidth (half width at half maximum) is obtained from the peak-to-peak linewidth of the derivative of the FMR absorption spectrum [Fig. 2(b)] using the formula,

$$\Delta H_{\mathrm{FW}} = \alpha f/|\gamma| + \Delta H_o, \quad \Delta H_{\mathrm{FW}} = \left(\frac{\sqrt{3}}{2}\right)\Delta H_{p-p}, \qquad (2)$$

where α is the net Gilbert damping, f is the microwave frequency, γ is the gyromagnetic ratio = 2.81 MHz/Oe [8,15], and ΔH_o is the intrinsic linewidth.

B. ISHE

For ISHE measurements, copper leads are attached as voltage electrodes on both ends of the sample using silver glue. The stripline antenna is isolated from the sample using a thin layer of polyimide.

IV. RESULTS AND DISCUSSION

A. Spin pumping and magnetic damping

First the damping and its enhancement by spin pumping are investigated on three samples, one reference sample S1:[bare YIG] and two samples covered by a spin sink material, namely, S2:[YIG/PEDOT:PSS] and S3:[YIG/Pt].

Figure 2(b) shows the FMR signal for YIG, YIG/Pt, and YIG/PEDOT:PSS at 8 GHz. The gray area indicates the

peak-to-peak linewidth. The increased linewidth for samples S2 and S3 indicates an increased damping.

By fitting the multiple lines of the resonance spectra using Lorentzian line shapes, the linewidths and H_{FMR} are obtained [see Fig. 2(c)]. The resonance peaks are defined according to the uniform mode position which is confirmed by extracting the saturation magnetization using the Kittel formula Eq. (3).

The damping is obtained by fitting the frequency dependence of the linewidth ΔH using Eq. (2) [13,15,25–28] and using the value of the gyromagnetic ratio γ estimated from the Kittel equation for the frequency dependence of H_{FMR} for the in-plane geometry,

$$\omega = 2\pi|\gamma|\sqrt{H_{FMR}(H_{FMR} + 4\pi M_{eff})}, \tag{3}$$

which yields $\gamma \sim 2.8\,\mathrm{MHz/Oe}$. The effective saturation magnetization estimated here is $4\pi M_{eff} = 1840\,\mathrm{Oe}$.

As a result we obtain $\alpha = 6.0 \pm 0.8 \times 10^{-5}$ for the bare YIG, $\alpha = 4.8 \pm 0.3 \times 10^{-4}$ for YIG/Pt, and $\alpha = 1.1 \pm 0.2 \times 10^{-4}$ for YIG/PEDOT:PSS [Fig. 2(d)]. The damping is enhanced by factors of ~2 and ~8 for YIG-PEDOT:PSS and YIG-Pt, respectively. This seems to be a strong indicator for spin pumping.

B. Magnetic damping control experiments

As mentioned above, enhanced damping can also have other origins. The net damping for the FM/conductor includes the contribution of all damping parameters,

$$\alpha_{net} = \alpha_{in} + \alpha_{sp} + \alpha_{eddy} + \alpha_{rad} + \alpha_{sh}. \tag{4}$$

This equation shows all damping contributions in a FM/conductor bilayer reported in literature. However, these contributions only occur under certain circumstances related to the properties of magnetic materials, waveguides, and experimental conditions. The strategy followed in our control experiments is to study every damping source individually by simultaneously excluding the other sources. For this purpose a series of control experiments is performed on additional YIG-based multilayers. These include the following samples: S4:[YIG/Al_2O_3], S5:[YIG/Al_2O_3/PEDOT:PSS], and S7:[YIG/Al_2O_3/Pt]. Sample S4 is intended to exclude any additional damping by the Al_2O_3 layer itself. Another group of samples is prepared to study the damping change with Pt thickness (5, 10, 15, and 20 nm) when an Al_2O_3 layer blocks the spin pumping. These samples are S6:[YIG/Al_2O_3/Pt(5)], S7:[YIG/Al_2O_3/Pt(10)], S8:[YIG/Al_2O_3/Pt(15)], and S9:[YIG/Al_2O_3/Pt(20)].

In samples S4, S5, and S7 the nonmagnetic and insulating Al_2O_3 layer prevents any spin injection from YIG into the nonmagnetic film. By blocking the spin current at the YIG/(NM,OC) interface we eliminate α_{sp}. So, the only damping enhancement in our YIG/Al_2O_3/(Pt,OC) will be due to the other damping effects which will be discussed later.

Before studying the enhanced damping in the YIG/Al_2O_3/(NM,OC) trilayers, we first test, in sample S4, whether the YIG/Al_2O_3 interface alone causes any additional damping. Figure 3(a) shows damping curves for samples S1 and S4. Obviously Al_2O_3 has no detectable influence on the damping. Although there is a nominal increase in damping it is only by approximately 10% and may well be related to small differences in the fit of the resonance lines and error bars. In the next control experiment we check whether the Al_2O_3 layer indeed blocks the spin pumping by investigating the ISHE in sample S7:[YIG/Al_2O_3/Pt]. Figure 3(b) shows the ISHE for sample S7 in comparison to sample S3. On the scale of the ISHE signal of sample S3 the plot clearly shows zero ISHE voltage, and, even for higher measurement sensitivity, no ISHE signal can be detected for sample S7. The Al_2O_3 layer thus efficiently suppresses any spin pumping. As a consequence any enhanced damping in samples S5 and S7 must have a different origin. Figure 3(c) shows the dependence of the linewidth on the frequency for samples S1, S2, and S5, respectively. Both samples with PEDOT:PSS show an identical increase in damping within the error bars. The inserted Al_2O_3 layer does not seem to have any influence. Nevertheless, the increase in damping is significant, approximately by a factor of 2. Figure 3(d) shows the linewidth/frequency dependence for samples S1, S3, and S7. Here we find that for the YIG/Al_2O_3/Pt sample the damping also is increased by a factor of ~2.5 with respect to bare YIG, a value comparable to sample S5. In contrast to the samples with PEDOT:PSS, however, the damping increase is much lower than for the direct YIG/Pt interface of sample S3. So, as a first result even without spin pumping we find a considerable increase in damping as soon as a conducting layer is placed on the sample.

As shown in Eq. (4) there are five possible contributions to the damping in FMR, α_{in} (intrinsic), α_{sp} (spin pumping), α_{eddy} (eddy currents), α_{rad} (radiative), and α_{sh} (shielding). The Gilbert damping constants considered here are α_{in}, α_{sp}, α_{rad}, and α_{sh}, whereas α_{eddy} is neglected. Eddy current damping α_{eddy} results from the eddy current generated in a conducting ferromagnetic material which is induced as a result of the magnetization precession. It depends on the conductivity of the FM, so it is negligible in magnetic insulators [12,16–18].

C. Radiation damping α_{rad} and electromagnetic shielding α_{sh}

Radiation damping α_{rad} is caused by the eddy currents induced in the waveguide [19–21]. As stated in Ref. [21] the waveguide and sample are designed for efficient excitation which in turn also means that the magnetization precession induces currents in the waveguide which lead to the increased damping. Unlike α_{eddy}, radiative damping depends on the properties and dimensions of the waveguide and the sample, so it is relevant for both ferromagnetic insulators and conductors. The damping contribution due to the radiation is given by

$$\alpha_{rad} = \frac{\mu_0^2 M_s \gamma \eta t \ell}{2 Z_0 W}, \tag{5}$$

where Z_0 and W are the conductor impedance and width, respectively, ℓ is the sample length, γ is the gyromagnetic ratio, and η is a dimensionless parameter that accounts for the mode profile in the sample [21]. It should be noted that the spacing between the waveguide and the sample also plays an important role. The radiative damping is decreased with increased spacing between the waveguide and the sample.

Especially in ferromagnets with very low damping, the contribution of radiation damping can become significant [29]. Because the effect is based on the coupling between the waveguide and the ferromagnet, it also contributes when

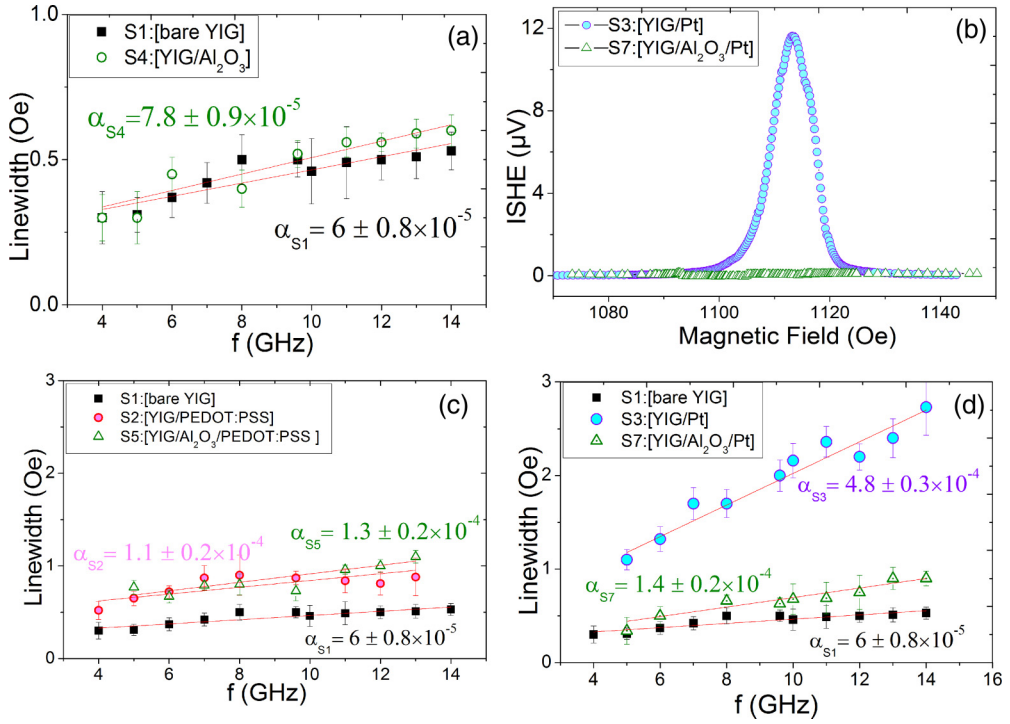

FIG. 3. Test of the suppression of the spin pumping by an Al_2O_3 interlayer. (a) An Al_2O_3 layer alone does not modify the damping of a single YIG film beyond the error bars. (b) In a YIG/Al_2O_3/Pt trilayer the ISHE is completely suppressed compared to a YIG/Pt bilayer. (c) Linewidth vs frequency plotted for pure YIG, YIG/PEDOT:PSS, and YIG/Al_2O_3/PEDOT:PSS. The damping enhancement due to PEDOT:PSS is significant, however, it is identical within the error bars with and without the insulating interlayer, respectively. (d) For the YIG/Al_2O_3/Pt an additional damping also is observed. Nevertheless, it is significantly smaller than without the Al_2O_3 interlayer.

we measure the damping of the pure YIG layer. So its magnitude must be smaller than the measured damping of $\alpha = 6 \pm 0.8 \times 10^{-5}$, and it can only be the cause of our findings if this coupling changes from sample to sample. We thus need to understand the influence of a thin conducting layer between the ferromagnet and the waveguide on the damping. Some publications also discuss the so-called electromagnetic shielding [22–24]. For example, Bailleul calculates that the presence of a thin conducting layer of sub-skin-depth thickness between the waveguide, and the ferromagnet effectively can shield the magnetic and electric fields and change the impedance of the waveguide [22]. A shielding of the field alone cannot increase the damping but will just decrease the amplitude. Nevertheless, a change in impedance can change the radiation damping as described in Eq. (5).

Our experimental findings can be explained by taking into account the interplay of radiation damping and the conducting layer which is used as a spin sink and which is in direct contact to the ferromagnet. Schoen *et al.* demonstrate that the spacing between the waveguide and the ferromagnet has a strong influence on the radiation damping [21]. For example, from direct contact between the waveguide and the ferromagnet to a spacing of 200 μm the radiation damping is decreased by two orders of magnitude. In our case the spacing between the waveguide and the ferromagnet is determined by the polyimide layer on the waveguide which has a thickness of tens of microns. However, when the conducting Pt or PEDOT:PSS layer is inserted it is in direct contact with the ferromagnet and hence reduces the spacing to zero. It can thus cause radiation damping by the eddy currents induced in the conducting layer by the inhomogeneous precession in YIG [Fig. 4]. Whereas for the pure YIG layer and large spacing, the radiation damping must be smaller than 6×10^{-5} an increase of only one order of magnitude in the case of the spin-pumping samples is enough to explain our findings and is in agreement with the results of Schoen *et al.* [21]. Also, our control samples with an Al_2O_3 interlayer fit this picture because the thickness of Al_2O_3 is only 30 nm. In this case, a radiation damping almost as large as for zero spacing can be expected. Furthermore, the different results for PEDOT:PSS and Pt are well in line with the theory of radiation damping. The resistance of the PEDOT:PSS layer (120 Ω)

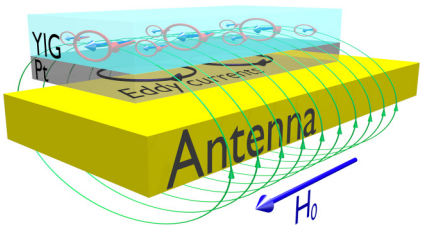

FIG. 4. Schematic for the measurement geometry during the FMR experiment. The rf field induced by the antenna causes an inhomogeneous precession in the YIG film. This precession induces eddy currents in the Pt layer which is located between the antenna and the YIG. Although the eddy currents induced by the antenna only reduce the amplitude of the signal, the eddy currents induced by the precession can cause additional damping and an increase in linewidth.

is approximately two times higher than the one for Pt (55 Ω). As a result the induced eddy currents and the related radiation damping are higher for the Pt-covered YIG than for the sample with PEDOT:PSS. From the measurements with the Al_2O_3 interlayer [Figs. 3(c) and 3(d)] we can determine the radiation damping by coupling to the conducting layer as the difference between the net damping and the damping in the bare YIG layer. For the Pt we obtain a value of $\Delta\alpha \approx 8\times10^{-5}$ and for the PEDOT:PSS $\Delta\alpha \approx 5\times10^{-5}$. It is noteworthy that these values are so small that they can barely be determined when using a metallic ferromagnet which often has a damping much higher than this. Only for the YIG layer, which exhibits a very low initial damping, can these values be measured accurately.

D. The net damping by spin pumping

So, in addition to the damping contribution by spin-pumping α_{sp}, any further damping enhancement for our ferromagnet/conductor stack can most likely be attributed to radiation damping α_{rad}.

If we want to determine the spin pumping we thus need to measure the difference in damping between the samples with YIG/Pt or YIG/PEDOT:PSS and the reference samples YIG/Al_2O_3/Pt and YIG/Al_2O_3/PEDOT:PSS, respectively [Figs. 3(c) and 3(d)]. For the Pt we find a difference of $\Delta\alpha \approx (3.4 \pm 0.4)\times10^{-4}$. For the PEDOT:PSS, however, there is no difference within the error bars. As a consequence we can conclude that any damping by spin pumping is extremely small and completely obscured by the radiation damping for PEDOT:PSS.

Because the additional damping associated with α_{rad} is caused by the current induced in the conducting layer capping the FM insulator, the damping also must depend on the resistance of the conducting layer. To investigate this issue we have fabricated a sequence of samples (S6–S9) consisting of YIG/Al_2O_3/Pt(x) trilayers with different Pt thicknesses x ($x = 5, 10, 15$, and 20) nm.

Figure 5(a) shows the frequency-dependent FMR linewidth for the different stacks, whereas Fig. 5(b) shows the pure radiation damping α_{rad} for the sample series S6–S9 obtained by measuring the total damping and subtracting the Gilbert damping of the single YIG layer. Except for sample S7, which shows an unexpectedly low damping, we observe a constant increase in damping with Pt thickness. We also have checked the sample resistances, and they scale inversely with Pt layer thickness. Table II shows the measured values for the damping and Pt resistance.

This contribution to the overall damping must also be considered when the results of spin-pumping experiments are used to calculate the spin-mixing conductance [11,25,30]. In the case of YIG/Pt the approximation of a spin-diffusion length in Pt smaller than the Pt thickness can be used, and the spin-mixing conductance can be calculated as follows:

$$g_{\uparrow\downarrow} = \frac{4\pi M_s t_{YIG}}{g\mu_B}\alpha_{sp}. \quad (6)$$

Using $t_{YIG} = 200$ nm, $4\pi M_s = 1531$ Oe, $g = 2.02$ [9], and $\mu_B = 9.27\times10^{-24}$ J/T [31], the resulting $g_{\uparrow\downarrow}$ is $6.8 \pm 0.8\times10^{18}$ m^{-2} if we do not correct for radiation damping.

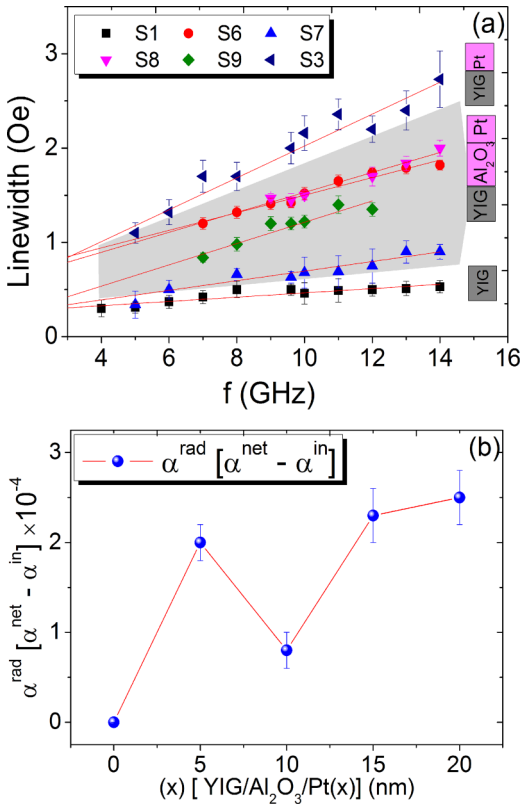

FIG. 5. (a) Linewidth vs frequency plotted for the sample sequence (S1, S6, S7, S8, S9, and S3). (b) The extracted radiation damping as a function of Pt thickness for the samples with 30 nm of Al_2O_3 between YIG and Pt.

If, however, we additionally consider a contribution by the radiation damping as measured with the Al_2O_3 interlayer the calculation yields $5.4 \pm 0.6\times10^{18}$ m^{-2}, which is a significant correction well beyond the error bars. It should be noted that both results are in the range of values reported in the literature [11,25,30]. Our calculations show that, even in systems with significant spin pumping, radiation damping can cause a large error. The influence of radiation damping has been reported in the literature, however, it was considered only as a correction for the intrinsic damping in the ferromagnet [21]. Its importance for spin-pumping experiments is mentioned here. The fact that with and without correction by radiation

TABLE II. Total damping α obtained experimentally for the YIG/Pt samples with and without Al_2O_3.

Sample	YIG/Al_2O_3 (30 nm)/Pt (x), x (nm)	Al_2O_3 (nm)-Pt (nm)	Damping α	R_{Pt} (Ω)
S1	YIG	0-0	$6.0 \pm 0.8\times10^{-5}$	
S6	YIG/Al_2O_3/Pt	30-5	$2.6 \pm 0.2\times10^{-4}$	200
S7	YIG/Al_2O_3/Pt	30-10	$1.4 \pm 0.2\times10^{-4}$	102
S8	YIG/Al_2O_3/Pt	30-15	$2.9 \pm 0.2\times10^{-4}$	91
S9	YIG/Al_2O_3/Pt	30-20	$3.1 \pm 0.3\times10^{-4}$	35
S3	YIG/Pt	0-10	$4.8 \pm 0.3\times10^{-4}$	55

damping our spin-mixing conductance for YIG/Pt lies within the values previously published by others [11,25,30] might be one additional reason for the deviations between different experiments.

For the polymer the situation is different. There the additional damping as measured [$\Delta\alpha \approx (0.5 \pm 0.2)\times 10^{-4}$] would result in a spin-mixing conductance of $8.0 \pm 3.2\times 10^{17}\,\mathrm{m}^{-2}$ if the approximation mentioned above was used. Most likely, however, the spin-diffusion length in PEDOT:PSS is larger than the PEDOT:PSS thickness [5] and a more complex formula needs to be applied [32] which also would necessitate measurements for different polymer thicknesses. As we show below, however, the extraction of the spin-mixing conductance is pointless. After correction for the radiation damping, no additional damping is left within the error bars. It should, however, be noted that the negligible increase in damping for the YIG/PEDOT:PSS interface does not mean that no spin pumping takes place. Most likely spins are injected into PEDOT:PSS creating a spin accumulation, however, due to the low spin-flip rate/long spin-diffusion length [5], the backflow is equally high. This way the steady-state spin current out of the ferromagnet which is the cause of the additional damping remains extremely small. In this case no comparison with past experiments is possible because no damping experiments have been reported for YIG/PEDOT:PSS.

From these results we must conclude that the spin-mixing conductance has to be calculated as

$$g_{\uparrow\downarrow} = \frac{4\pi M_s t_{\mathrm{YIG}}}{g\mu_B}(\alpha_{NM} - \alpha_{FM} - \alpha_{\mathrm{rad}}), \tag{7}$$

where, α_{NM}, α_{FM}, and α_{rad} are the damping as measured for the combination of ferromagnet and spin sink, the intrinsic damping for the FM only, and the radiation damping, respectively.

The fact that for PEDOT:PSS we find mainly radiation damping and no indication of spin pumping beyond the error margins is in agreement with the low spin-orbit coupling expected for organic materials. As a further control experiment, we perform a measurement of the ISHE on a YIG/PEDOT:PSS sample. The experiment is performed in a way similar to the measurement on YIG/Pt shown in Fig. 3(b). Nevertheless, after carefully excluding artifacts we only find an ISHE voltage of approximately 3 nV [Fig. 6]. Despite the fact that the resistance of PEDOT:PSS is more than twice as high as the one of the Pt film, the ISHE is more than three orders of magnitude lower. This nicely confirms either very low spin pumping or at least very low spin scattering in the polymer in agreement with the weak spin-orbit coupling, long spin-diffusion length, and very low spin Hall angle for these kinds of materials [5,26–28].

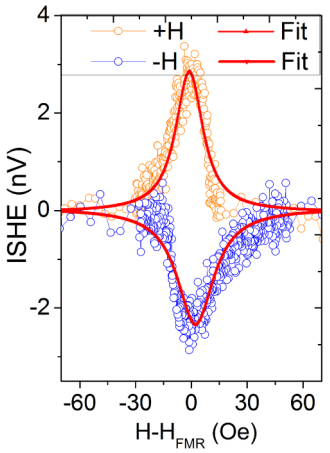

FIG. 6. The ISHE for YIG/PEDOT:PSS for in-plane geometry and both magnetic-field polarities $+H$ and $-H$. The curves are fitted using a Lorentz fit. The ISHE voltage is as small as ∼3 nV.

V. CONCLUSION

Our results show that, when ferromagnetic layers with very low damping are used for spin-pumping experiments, radiation damping may be a major part of the total damping. In spin-pumping experiments, the conducting spin sink which is deposited on the ferromagnet's surface adds damping just by eddy currents which are induced due to inhomogeneous precession in the ferromagnet. Especially, when a spin sink with low spin scattering (such as organic materials) and thus low damping enhancement is investigated, the radiation damping can yield results which are bigger than any damping stemming from the spin pumping itself. Because the radiation damping is difficult to estimate, it is necessary to perform experiments on reference samples with nonconducting interlayers which inhibit the spin pumping. These allow for measuring the radiation damping directly which can then be used to correct the values obtained for the spin-pumping samples without interlayers.

ACKNOWLEDGMENTS

This work was funded by the Deutsche Forschungsgemeinschaft (DFG) through Grant No. SFB 762 "Functionality of Oxide Interfaces" TP B9 and by the "Deutscher Akademischer Austauschdienst (DAAD)."

[1] K. Ando, S. Takahashi, J. Ieda, Y. Kajiwara, H. Nakayama, T. Yoshino, K. Harii, Y. Fujikawa, M. Matsuo, S. Maekawa, and E. Saitoh, J. Appl. Phys. **109**, 103913 (2011).

[2] K. Uchida, S. Takahashi, K. Harii, J. Ieda, W. Koshibae, K. Ando, S. Maekawa, and E. Saitoh, Nature (London) **455**, 778 (2008).

[3] G. E. W. Bauer, E. Saitoh, and B. J. van Wees, Nat. Mater. **11**, 391 (2012).

[4] J. Xiao, G. E. W. Bauer, K. Uchida, E. Saitoh, and S. Maekawa, Phys. Rev. B **81**, 214418 (2010).

[5] K. Ando, S. Watanabe, S. Mooser, E. Saitoh, and H. Sirringhaus, Nat. Mater. **12**, 622 (2013).

[6] D. Sun, K. J. van Schooten, M. Kavand, H. Malissa, C. Zhang, M. Groesbeck, C. Boehme, and Z. Valy Vardeny, Nat. Mater. **15**, 863 (2016).

[7] Y. Tserkovnyak, A. Brataas, and G. E. W. Bauer, Phys. Rev. Lett. **88**, 117601 (2002).

[8] Y. Kajiwara, K. Harii, S. Takahash, J. Ohe, K. Uchida, M. Mizuguchi, H. Umezawa, H. Kawai, K. Ando, K. Takanashi, S. Maekawa, and E. Saitoh, Nature (London) **464**, 262 (2010).

[9] B. Heinrich, C. Burrowes, E. Montoya, B. Kardasz, E. Girt, Y.-Y. Song, Y. Sun, and M. Wu, Phys. Rev. Lett. **107**, 066604 (2011).
[10] Y. Sun and M. Wu, Solid State Phys. **64**, 157 (2013).
[11] H. L. Wang, C. H. Du, Y. Pu, R. Adur, P. C. Hammel, and F. Y. Yang, Phys. Rev. Lett. **112**, 197201 (2014).
[12] B. Heinrich, R. Urban, and G. Woltersdorf, J. Appl. Phys. **91**, 7523 (2002).
[13] T. Liu, H. Chang, V. Vlaminck, Y. Sun, M. Kabatek, A. Hoffmann, L. Deng, and M. Wu, J. Appl. Phys. **115**, 17A501 (2014).
[14] C. Hauser, T. Richter, N. Homonnay, C. Eisenschmidt, M. Qaid, H. Deniz, D. Hesse, M. Sawicki, S. G. Ebbinghaus, and G. Schmidt, Sci. Rep. **6**, 20827 (2016).
[15] H. Chang, P. Li, W. Zhang, T. Liu, A. Hoffmann, L. Deng, and M. Wu, IEEE Magn. Lett. **5**, 6700104 (2014).
[16] M. Charilaou, K. Lenz, and W. Kuch, J. Magn. Magn. Mater. **322**, 2065 (2010).
[17] J. M. Lock, Br. J. Appl. Phys. **17**, 1645 (1966).
[18] I. S. Maksymov, Z. Zhang, C. Chang, and M. Kostylev, IEEE Magn. Lett. **5**, 3500104 (2014).
[19] R. W. Sanders, D. Paquette, V. Jaccarino, and S. M. Rezende, Phys. Rev. B **10**, 132 (1974).
[20] G. Wende, Physica Status Solidi A **36**, 557 (1976).
[21] M. A. W. Schoen, J. M. Shaw, H. T. Nembach, M. Weiler, and T. J. Silva, Phys. Rev. B **92**, 184417 (2015).
[22] M. Bailleul, Appl. Phys. Lett. **103**, 192405 (2013).
[23] M. Kostylev, J. Appl. Phys. **106**, 043903 (2009).
[24] I. S. Maksymov and M. Kostylev, J. Appl. Phys. **113**, 043927 (2013).
[25] M. Haertinger, C. H. Back, J. Lotze, M. Weiler, S. Geprägs, H. Huebl, S. T. B. Goennenwein, and G. Woltersdorf, Phys. Rev. B **92**, 054437 (2015).
[26] M. Kimata, D. Nozaki, Y. Niimi, H. Tajima, and Y. C. Otani, Phys. Rev. B **91**, 224422 (2015).
[27] S. Watanabe, K. Ando, K. Kang, S. Mooser, Y. Vaynzof, H. Kurebayashi, E. Saitoh, and H. Sirringhaus, Nat. Phys. **10**, 308 (2014).
[28] J. B. S. Mendes, O. Alves Santos, J. P. Gomes, H. S. Assis, J. F. Felix, R. L. Rodríguez-Suárez, S. M. Rezende, and A. Azevedo, Phys. Rev. B **95**, 014413 (2017).
[29] M. A. W. Schoen, D. Thonig, M. L. Schneider, T. J. Silva, H. T. Nembach, O. Eriksson, O. Karis, and J. M. Shaw, Nat. Phys. **12**, 839 (2016).
[30] S. M. Rezende, R. L. Rodríguez-Suárez, and A. Azevedo, Phys. Rev. B **88**, 014404 (2013).
[31] *Ultrathin Magnetic Structures I: An Introduction to the Electronic, Magnetic and Structural Properties*, edited by J. A. C. Bland and B. Heinrich (Springer, Berlin, Heidelberg, 2006), Vol. 1.
[32] Y. Tserkovnyak, A. Brataas, and G. E. W. Bauer, Phys. Rev. B **66**, 224403 (2002).